Materials Today Communications 40 (2024) 109428

Contents lists available at ScienceDirect

Materials Today Communications

journal homepage: www.elsevier.com/locate/mtcomm

Electrophoretic deposition of TiO_2 nanotubes and antibiotics on polyurethane coated stainless steel for improved antibacterial response and cell viability

Fabiola A. Gutiérrez-Mejía [a], Claudia Vásquez-López [a], Rossana F. Vargas-Coronado [a], Fabiola E. Villa-de la Torre [b], Víctor E. Arana-Argaez [b], Ingrid M. Rodríguez-Buenfil [c], María M. Gamboa-Angulo [a], Yadir Torres [d,*], Juan V. Cauich-Rodríguez [a]

[a] Centro de Investigación Científica de Yucatán, Calle 43 # 130 ×32 y 34, Colonia Chuburná de Hidalgo, C.P. 97205, Mérida, Yucatán, Mexico
[b] Facultad de Química, Universidad Autónoma de Yucatán, Calle 43 ×90, núm. 613, col. Inalámbrica, CP 97069, Mérida, Yucatán, Mexico
[c] Centro de Investigación y Asistencia en Tecnología y Diseño del Estado de Jalisco, A.C. Tablaje Catastral 31264 Km 5.5 Carr. Sierra Papacal – Chuburná Puerto. Parque Científico Tecnológico de Yucatán. C.P.97302. Mérida, Yucatán, Mexico
[d] Departamento de Ingeniería y Ciencia de los Materiales y del Transporte, Universidad de Sevilla, Calle Virgen de África 7, 41011, Sevilla, Spain

ARTICLE INFO

Keywords:
Electrophoretic deposition
Anatase
Nisin
Gentamicin
Polyurethane
Coatings

ABSTRACT

In the quest for advancing the performance of metallic implants, surface modification emerges as a pivotal strategy to mitigate ion depletion, enhance the host's biological response, and exhibit anti-microbial behavior with reduced cytotoxicity. In this study, we developed a non-traditional electrophoretic deposition (EPD) hybrid coating for medical-grade stainless steel 316 L (SS316L) surfaces covered with a segmented polyurethane (SPU). These coatings are composed of anatase TiO_2 nanotubes (TiO_2_A), and antibiotics (nisin N or gentamicin G). We characterized the modified metals using FTIR and Raman spectroscopy, contact angle measurements, AFM, TGA, SEM-EDX, as well as assessing their antimicrobial response and cell cytotoxicity. The results demonstrate the formation of porous surfaces with embedded nanotubes and antibiotics within and on the polyurethane surfaces. Samples with SPU+ TiO_2_AG EPD exhibited superior coverage, antimicrobial properties, and enhanced viability compared to cases where only particles or antibiotics were coated individually. Additionally, samples of SPU+ TiO_2_AN EPD displayed favorable hydrophilicity and suitable cytotoxicity. Therefore, the synergistic effect of nanoparticles and antibiotics positively influences the functionality of the coating.

1. Introduction

Metals find extensive applications in the field of medical implants owing to their exceptional mechanical strength and chemical stability. In particular, medical grade stainless steel (SS) emerges as a favorable choice in the manufacturing of osteosynthesis plates and screws, commonly utilized for the correction of bone tissue fractures [1]. The predilection of SS respect other metals (titanium and titanium alloys) relies in its cost-effectiveness and superior mechanical resistance.

Although biocompatible, SS faces suboptimal bone and tissue bonding due to a tenfold stiffness compared to human bones [2]. SS is particularly susceptible to corrosion and release of harmful metal ions for prolonged periods of implantation, as some works report a high incidence of corrosion in SS implanted pieces (> 70 %) [3,4]. Additionally, the lack of inherent antimicrobial properties, might complicate the heal of possible infections occurred during surgery and eventually impede a smooth assimilation of the implant [2,5]. Another problem involves SS bio inertness, which greatly limits the implant's osteointegration capacity with bone and surrounding tissue.

Several proposals from the material community have been raised to improve the biocompatibility of metallic implant surfaces. One of the approaches include surface treatments, either physical [6,7] or chemical [8,9]. Among the reported physical methods there is the grit-blasting, consisting of the induction of roughness of metal surfaces by spraying at high velocity particles of alumina, silica, or titanium dioxide [10]. Laser ablation and patterning is another physical method explored mainly for dental implant applications; an asset of this method is the high tunability of the technique [11]. Other physical methods are

* Corresponding author.
E-mail address: ytorres@us.es (Y. Torres).

https://doi.org/10.1016/j.mtcomm.2024.109428
Received 27 March 2024; Received in revised form 16 May 2024; Accepted 31 May 2024
Available online 8 June 2024

plasma coating and glow discharge ion implantation which not only are meant to improve the biocompatibility of the metals but also to improve their mechanical properties and resistance to corrosion [7]. Chemical methods comprise acid or alkali etching which have shown excellent results in bone adhesion and osteoblast proliferation [12].

Surface coatings, especially those based on bioactive glass [13], biopolymers [14,15] or hydroxyapatite [16], have become crucial in improving biocompatibility since they facilitate the adhesion of the biological entities and trigger bioactive responses. Other strategies have made use of the addition of nanoparticles (metallic and non-metallic) [17–19], peptides [20] and antibiotics [21] which are being explored for prevention of nosocomial infections that are considered the main complications of medical implants [22,23].

Several techniques are being developed for deposition of polymers, particles, and biomolecules onto metallic surfaces [24,25]. Among these techniques, electrospinning, sputtering, dip coating, and electrophoretic deposition have received considerable attention [24–26].

Electrophoretic deposition (EPD) is a versatile technique that allows the incorporation of polymers and particles either individually or simultaneously. Additionally, EPD enables the formation of homogeneous coatings and layers of controlled thickness onto (mainly) metallic surfaces [27–30]. Some of the advantages of EPD are that operates at room temperature, allows the coating on irregular surfaces, is compatible with biological entities (cells, proteins, etc.) and uses accessible lab equipment. Since EPD coatings adhere directly to metals, it is an excellent method to produce coating for medical implants. For example, EPD was used to deposit alginate/bioglass on magnesium alloys [31] where the authors found out an improvement in the bioactivity of the coated implant. Also, hydroxyapatite (HA)/Chitosan deposited by EPD on titanium substrates exhibited excellent cell adhesion and proliferation [32]. Many more examples can be found in literature with medical metals coated with EPD where the biocompatibility is improved in contrast with bare metals [33,34]. An additional feature that can be implemented with EPD is the antibacterial function. Bocaccini *et al.* [35] reviewed the state of art about in this respect and describes the main bacterial mechanisms of EPD coating in four stages/steps: 1) release of antibiotics, 2) death by direct contact with the surface, 3) stimuli-response killing 4) antifouling coating towards bacteria.

In this context, it is proposed a hybrid coating of SS316 L metallic substrates that addresses the potential problems of corrosion, poor osseointegration and bacterial hosting. For this purpose, a layer of polyurethane was loaded with TiO_2 nanotubes and antibiotics by EPD. We were inspired in the multiple works in literature that use EPD to achieve hybrid multifunctional coatings onto metals [36–39]. These materials were used considering their known medical application. Segmented polyurethanes like Tecoflex SPU are widely used in the biomedical field for a variety of devices such as catheters, cardiac valves, dialysis membranes, even as pacemaker lead and stent coating [40,41]. This aliphatic polyether-based thermoplastic medical grade polyurethane can be applied by extrusion, injection or even in solution and can be formulated with radiopacifiers for a better follow up. Although SS316L is expected not to corrode easily, the presence acidic media, saline solutions, high voltages, typically used in EPD and continuous use in biological media might leads to degradation. Therefore, SPUs can provide a suitable cover to SS316L to prevent erosion and possibly corrosion while softening the contact surface. There exists a body of literature supporting the efficacy of coatings in enhancing corrosion resistance across different metal substrates [42–44].

Furthermore, TiO_2 nanoparticles, especially as anatase, possess antibacterial and antiproliferative properties so they can be used as additive in medical devices [45]. The deposit of titania nanotubes on a SPU coated SS is expected to enhance tissue-implant interaction as reported in nanostructured titania coatings on 99.5 % titanium substrates [46] or to prevent orthopedic implant infections on titanium plates coated with TiO_2 nanotube arrays with planar TiAg [47]. TiO_2 nanostructures (nanofibers, nanoneedles and nanowires) were found to provide suited topographies to host fibroblasts and to have photoactive antibacterial properties [48]. Nisin is a peptide that has been mainly considered as a food preservative [49] but thanks to its bactericide properties, especially for gram positive bacteria, it has only recently been studied as a safe additive for dental caries and other medical applications [50–52]. More recently, it has been used to modify Ti6Al4V-ELI alloy to reduce the risk of peri-implant infections [53].

Gentamicin is a broad-spectrum aminoglycoside antibiotic with applications on treatments of septicemia, meningitis, urinary tract infections and intestinal tract infections, among others [54] and widely used in bone cement formulations. However, there are a few studies on gentamicin deposition by EPD [27].

This study offers a comprehensive physicochemical characterization of the EPD coatings, and an examination on the influence of porosity, contact area, and interactions with cellular and bacterial entities. In essence, this work constitutes an exploration of the capabilities of Electrophoretic Deposition (EPD) for the development of hybrid coatings, with particular relevance to potential applications in the realm of biomedical metallic implants.

2. Material and methods

Chloroform was purchased from J.T Baker (NJ, USA) whereas the antibiotics (Gentamicin sulphate and Nisin) were purchased from Sigma Aldrich (MO USA) and Silver-Elephant BIO-ENGINEERING CO., LTD, (Zhejiang, China) respectively. Polyurethane Tecoflex™ SG 80 A was obtained from Lubrizol (Ohio, USA). The 316 L medical grade stainless steel metal (SS316 L) plates (15 cm × 15 cm) were purchased from Jindong Store (Beijing, China). Metallic coupons were cut and shaped inhouse in circles of 14 mm diameter with a small edge for electrical connection. Metal coupons were ground with 60 grit sandpaper and subsequent finer grit with 280 sandpaper with an average surface roughness of 0.53±0.21 μm.

Titanium dioxide nanotubes (TiO_2_A) used in this study were supplied by Petropipe (Veracruz, México). These particles were used as received where large agglomerates were observed by SEM (see supplementary information S1). EDX analysis also showed that they contained carbon in their composition as shown in the S2 section of the supplementary information. These particles possess filament shape and have an approximate width of 50± 20 nm with approximate lengths 760 ± 120 nm. Crystalline phase of nanotubes is anatase according to Raman spectroscopy.

2.1. Substrate preparation and electrophoretic deposition

Polyurethane coated SS316L was prepared first by dissolving Tecoflex (SPU) in chloroform at a concentration of 50 mg/ml. Stainless steel coupons were dipped in the chloroform-SPU solution twice during 3 s with a waiting interval of 10 min, then samples were dried at 25 °C for 48 hours. TiO_2 nanotubes at a concentration of 1.25 mg/ml were dispersed in deionized water and then the pH adjusted to 3 using acetic acid. Then, antibiotics were added, at a concentration of 1 mg/ml. The mixtures of nanotubes/antibiotics were placed in an ultrasonic bath for 30 min and then continuously stirred to ensure that the particles were homogeneously dispersed. Fresh solutions were used after each deposition. Thickness of layers was measured before and after deposition using a Mitutoyo 547–500 S Digital Thickness Gauge with Flat Anvil.

Electrophoretic deposition was conducted by using a direct voltage source (MPS-6005 L-1, MATRIX, China). The working cell consisted of a bare SS316 L anode and a cathode of Tecoflex coated SS316 L separated at a fixed distance of 8 mm. Electrodes were immersed in the mixture containing TiO_2 and antibiotics and a voltage of 25 V was applied for 3 min. After that the samples were dried at room temperature for at least 48 hours. Several samples were produced as needed for each analysis. The following notation was employed (see Table 1) for prepared samples. It is important to mention that despite the low zeta potential of

Table 1
Notation used for samples. **Note:** Voltage = 25 V and Time = 3 min.

Solution	Notation*
water	SPU EPD
1.25 mg/ml nanotubes	SPU+TiO_2_A EPD
1.25 m/ml nanotubes + 1 mg/ml nisin	SPU+ TiO_2_AN EPD
1.25 m/ml nanotubes + 1 mg/ml gentamicin	SPU+ TiO_2_AG EPD
1 mg/ml of nisin	SPU+ N EPD
1 mg/ml of gentamicin sulphate	SPU+ G EPD

* When EPD does not appear in the sample name it means that no EPD treatment was employed. When no SPU appears in the sample name it means that experiments were applied on bare SS316L

titanium dioxide nanotubes, the high electrical resistance of the SPU coating and voltage and time, these conditions were used to avoid hydrolysis considering the high salt content of nisin during EPD.

2.2. Physicochemical characterization

A NANO ZEN3600 setup (Malvern, Worcestershire, UK) was used to determine the parameters of the TiO_2 suspensions (Size, Z-potential) at room temperature. The electrophoretic mobility and Z potential of titanium dioxide nanotubes (TiO_2_A), was determined at different pH with a concentration of 1 mg/ml. Each zeta value represented an average for three different measurements.

FTIR spectra were recorded using a Thermo Scientific Nicolet 8700 (MA, USA) spectrometer. Attenuated total reflectance (ATR) FTIR was obtained in the 4000 and 650 cm^{-1} (or 600 cm^{-1}) spectral range averaging 100 scans with a resolution of 4 cm^{-1}. Raman spectra was acquired using an inVia Renishaw Raman spectrometer (IL USA). The system collected a Raman shift spectral range of approximately 3200–100 cm^{-1}. A 633 nm argon laser was used as the excitation radiation source.

In addition, the morphology of the surfaces was assessed by using a SEM JSM 6360 LV or a SEM JSM-7601 F (JEOL, Tokio, Japan) setup with acceleration voltage of 20 kV. Microanalysis mapping and composition analysis were conducted with Energy-dispersive X-ray spectroscopy (EDX) (INCA X-sight Model 7582, Oxford Instruments). To study the topography (height and phase) of samples, Atomic Force Microscope (AFM) Bruker Innova IRIS (MA, USA) setup was used in tapping mode. Software Gwyddion was used to measure AFM parameters, Rq was determined for several areas on the polyurethane, in this case, holes were excluded. To analyze AFM phase contrast measurements, Image J software was employed with the Analyze particles plugin.

To estimate the surface density and mass of coatings, a thermogravimetric analysis was conducted. Mass loss and residual mass percentage was calculated using a TGA-7 from Perkin-Elmer (CT, USA). Samples of known initial mass were heated from 50 ℃ to 700 ℃ at 10 C/min under nitrogen atmosphere. Metal coupons with the deposits were peeled (since the small scale only allows few mg samples) and a fraction of the coating was weighted for posterior analysis. From the initial and residual masses of SPU and TiO_2_A measured separately, a % of survival= mf/m0 was obtained. Then the mass fraction of TiO_2 nanotubes was determined in samples of SPU+TiO_2_A.

To measure the wettability of our samples, contact angle measurements were performed. A Ramé-hart model goniometer/tensiometer was used, in combination with DropImage Advanced v2.8 software. Static contact angle measurements were made by sessile drop method using deionized water on the prepared surfaces at room temperature. Three samples were measured at an interval of 10 s from the droplet deposit.

2.3. Antimicrobial susceptibility assay

Staphylococcus aureus (ATCC- 25923) and wild type *E. coli* strains were used for our susceptibility assays. A Kirby-Bauer disc diffusion method in the pour plate mode [55] was implemented. Bacteria were cultured in a Muller-Hinton medium, and the concentration of bacteria was adjusted to 0.5 in the Mc Farland scale equivalent to 1×10^8 CFU/ml. Finally, 1.7 ml of the bacterial solution was added to 168.3 ml of Muller-Hinton Agar to achieve a 100X dilution. Samples were sterilized with UV light, placed on 150 mm petri dishes, and covered with approximately 55 ml of inoculated agar. Petri dishes were incubated for 24 h at 37 °C and the inhibition halo was checked. To contrast the inhibitory halos of EPD deposited samples, reference samples were prepared by simple adsorption on SS316 L coupons covered with SPU. Briefly, TiO_2_A, gentamicin and nisin were dissolved in water and pH adjusted to 3 with acetic acid. Then, 100 μl of 1 mg/ml solutions of TiO_2_A, gentamicin and nisin were incubated (100 μg) on coupon triplicates and left to evaporate at room temperature for 48 h. In reference samples, the EPD suffix does not appear in the sample name.

2.4. Resazurin cell viability

Cytotoxicity was assessed using human fibroblasts (Detroit 548 ATCC, CCL-116, American Type Culture Collection, Rockville, MD, USA). Extracts of the materials were obtained for indirect cytotoxicity tests. SS316L disks were plated in sterile 48-well plates with low glucose Dulbecco's Modified Eagle's Medium (DMEM) culture medium (Caisson Laboratories, Smithfield, UT) supplemented with 10 % fetal calf serum (Biowest) and streptomycin/ 1 % penicillin (Sigma Aldrich), at 37°C and 5 % CO_2 following a ratio of 1 disk per 1.5 ml of medium. The effect of the extracts was evaluated by seeding CCL-116 in a 96-well plate to a density of 1×10^4 cells per well in 100 μl of supplemented culture medium. Four wells were used as positive control. After 24 h, the medium was removed and the extracts were added to the cells, followed by further incubation for 24, 48, and 72 h. Consequently, its viability was evaluated by measuring the reduction of Resazurin. The absorbance of the samples was measured using a Cytation 3 plate reader (Biotek) at 570 and 600 nm. Data are expressed as percentages of viability. After 24 hours of incubation, the extracts were tested with the cell culture. Absorbance was recorded at 24, 48 and 72 hours. To contrast the viability of EPD prepared samples, reference samples were prepared by simple adsorption on SS316 L coupons coated with SPU as reported before. Briefly, TiO_2_A, gentamicin and nisin were dissolved in water and pH adjusted to 3 with acetic acid. Then, 100 μl of 1 mg/ml suspensions of TiO_2_A, gentamicin and nisin were incubated (100 μg) on coupon triplicates and left to evaporate at room temperature for 48 h. In reference samples, the *EPD* suffix does not appear in the sample name.

To calculate the viability % the following equation was used:

$$\% \quad \nu \quad = \frac{(O_2 - A_1) - (O_1 - A_2)}{(O_2P_1 - O_1P_2)}$$

Where:

O1 = molar extinction coefficient € of oxidized alamar Blue (blue) at 570 nm = 80586

O2 = E of oxidized alamar Blue at 600 nm = 117216

A1 = absorbance of test wells at 570 nm

A2 = absorbance of test wells at 600 nm

P1 = absorbance of positive growth control well (cells plus alamar Blue but no test agent) at 570 nm

P2 = absorbance of positive growth control well (cells plus alamar Blue but no test agent) at 600 nm

As indicated by the supplier [56]. The average and the standard deviation of the viability % was calculated from four samples.

2.5. Statistical analysis

An ANOVA test was implemented to compare the cell viability obtained from the extracts of our samples against the control SPU sample. A Tukey test was used with a confidence level of 95 % ($p<0.05$) using

the software Origin 8.5.

3. Results and discussion

The working principle of EPD relies on the application of an electric field in a suspension of well-dispersed charged particles (in this case nanotubes) which migrate towards the electrode of opposite charge [57]. For example, if the net charge of particles in the suspension is positive, they will migrate towards the cathode (negative electrode), this configuration is considered cathodic EPD (cEPD). Accordingly, a cathodic electrophoretic deposition cEPD was implemented as shown in Fig. 1a.

There are several factors that influence the deposition yield; namely, the solvent used, the stability of the suspension, the voltage applied (AC or DC) and the time of actuation.

It is considered that good stability is achieved for ZP>±30 mV. To investigate the stability of the suspensions, the zeta potential (ZP) was measured as a function of pH (see Fig. 1b). ZP of nanotube suspensions is negative for pHs above 4 and becomes positive around pH 3 (ZP = 2.8 ±0.7 mV) and below. When antibiotics are added to the suspensions the ZP increases towards positive values: 10.1±0.4 mV and 25.4±0.5 mV for gentamicin and nisin respectively. Additionally, it is reported that in acidic media both antibiotics are stable [58,59]. Due to an increase of electropositivity in antibiotics-nanotubes suspensions, the cEPD experiments were performed at pH 3. It would be of interest to investigate deposit yields depending on pH, especially at pH > 5 in which an anodic deposition would take place. In such cases suspensions of TiO_2 nanotubes are more stable but there would be a counterbalance effect due to the addition of antibiotics.

Water might not be a preferred solvent in terms of electrophoretic mobility and deposition yield, respect other polar solvents such as ethanol, acetone, isopropanol, etc. [60–62]. These solvents caused swelling and degradation of the SPU layer and SPU detachment from the electrode in our setup. Another aspect to consider was the stability of the biomolecules, in the suspension particles-antibiotics TiO_2_AN and TiO_2_AG as electrolysis was observed in addition to agglomeration. To minimize these effects the actuation time was reduced to 3 min and the voltage set at 25 V in agreement to other literature works (1–30 V, 1–5 min, water solvent w/acetic acid). For example, Aydemir *et al.* [37] applied 18 V for 5 min for EPD coatings on SS316L chitosan/gelatin/silica-gentamicin. An aspect to highlight is the fact that the SPU is a nonconductive material, which might cause a reduction in the yield of deposits. From Fig. 1c, it can be observed a layer of hybrid coating with whiteish blots (being the SPU layer almost transparent) and by zooming in (40X) with a traditional optical microscope, we can observe the presence of agglomerates of clusters of particles/antibiotics.

Another significant aspect is the resistance to corrosion provided by the SPU coating. For this, preliminary electrochemical experiments were conducted and included in the supplementary information, (see section S3). The information about the pitting potential, corrosion rate and the difficulty of self-repair of the passive film can be obtained by potentiometric cyclic polarization curves (Figure S3b). Measurements indicate that coated SPU SS316L, relative to bare SS316L specimens, exhibited decreased passive current densities. Being the current densities in the order of 10^{-12} to 10^{-8} mA/cm^2 for SS316L and 10^{-9} to 10^{-2} mA/cm^2 for SPU SS316L. Therefore, in the event of corrosion, the rate would be at least three orders of magnitude slower in the SPU coated sample than the bare metal. The polarization curve of SS316L sample shows the characteristic kink indicating the breakdown of the passive layer, giving place to stable pitting corrosion [63]. The pitting potential of SS316L sample Ep occurs at ≈70 mV. In the case of the SS316L+SPU there is no indication of breakdown of the passive layer even in potentials above the Ep of SS316L. Furthermore, the hysteresis loop in sample SPU+SS316L is negative, i.e. the current density of the reverse scan is less than the current density of the forward scan, meaning that no irreversible damage occurs at the electrode surface. In contrast, sample SS316L exhibits positive hysteresis where the current density of the reverse scan exceeds the forward scan's current density, this behavior indicates undergoing pitting corrosion [64]. Therefore, the SPU layer does not favor pitting corrosion in our experiments. Yet, a thorough examination of corrosion remains a fundamental aspect for further studies. The feasibility of implementing a non-conductive layer on a metallic electrode has been

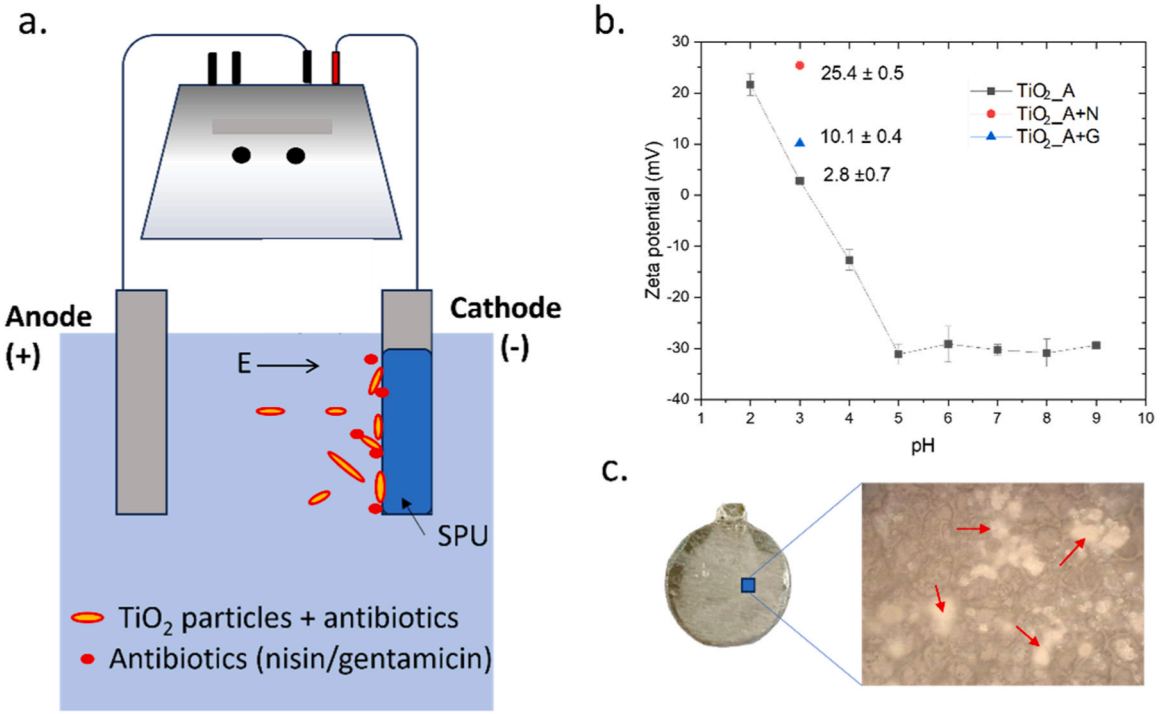

Fig. 1. **a**. Diagram of the electrophoretic deposition setup **b**. Zeta potentials of TiO_2_A suspensions at different pH values ranging from 2 to 9 (mean ± SD, n = 3). **c**. Photo and micrography of a SS 316 L coupon with TiO_2_A nanotubes and gentamicin.

demonstrated before [65–67] where carbon nanotubes have been deposited on rubber, silicon and ceramics. To our knowledge, the work presented here is the first report in which a SPU covers a metallic electrode and EPD is used for coating, all in the context of medical implants.

FTIR spectra of raw materials and modified surfaces are shown in Fig. 2a. Spectrum of gentamicin sulphate (G) shows characteristic peaks reported previously in literature. [68] The bands at 3423 and 2960 cm^{-1} correspond to N-H and C-H stretching vibrations respectively. The absorption bands at 1619 and 1520 cm^{-1} can be ascribed to the N-H bending of the amides (I and II respectively) in the aminoglucoside. The band at 1124 indicates HSO_4 vibration while absorptions at 1042 and 619 cm^{-1} indicate S-O bending as reported in [69]. Nisin FTIR (N) shows bands at 3386 and 2965 cm^{-1}which are attributed to O-H and N-H stretching. The bands at 1648 and 1536 cm^{-1} are assigned to primary and secondary amides. TiO_2_A spectra showed features reported elsewhere for anatase. [70] A broad band around 3465 cm^{-1} is indicative of stretching of OH groups, the band at 1641 is related to the bonds Ti-OH of water absorbed in the nanotubes; a band related to Ti–O–Ti bonds is expected between 400 and 600 cm^{-1} bands, but it was not observed as this interval was not recorded due to the ATR technique. SPU spectrum exhibits multiple peaks in accordance with previous results in literature [71] i.e. the band at 3326 cm^{-1} relates to NH stretching while bands between 2936 and 2854 cm^{-1} relate to CH_2 stretching; the peak at 1719 indicates C═O stretching in urethanes and the band at 1533 reveals C-N+N-H bond bending; finally, the intense band at 1100 shows asymmetric C-O-C (polyether) stretching. Spectra of SPU+TiO_2_AN and SPU+TiO_2_AG showed absorptions mainly corresponding to the SPU phase due to the low number of deposits.

Raman spectroscopy was also used to identify components on the surface (see Fig. 2b). In this regard, gentamicin shows an intense absorption at 977 cm^{-1} related to C-O-C stretching as reported previously. [72] Nisin spectra showed high fluorescence and is not included here due to signal saturation; however, N-H stretching band near ~3270 cm^{-1} and peaks located near ~1656 and ~1537 cm^{-1} assigned to Amide I and Amide II has been reported in literature.[73] TiO_2_A nanotubes exhibited anatase spectra features [70,74] where peaks at 153, 195, 393, 509 and 635 cm^{-1} are observed. SPU signal also showed main bands at 2919 and 2860 cm^{-1} corresponding to CH stretching, whereas peak at 1436 cm^{-1} relates to aliphatic CH_2 bending while the 1296 cm^{-1} peak is attributed to the C-O and C-N stretching. [75] Spectra of both SPU+TiO_2_AN and SPU+TiO_2_AG showed peaks corresponding to the SPU and to the TiO_2_A nanotubes. However, SPU+TiO_2_AG exhibited a small peak at 977 cm^{-1} demonstrating gentamicin presence.

As mentioned earlier Tecoflex SPU was chosen since it is widely used in the biomedical field. Prior to EPD, SS316 L was coated with layers of SPU by fast evaporation method. On average (n=20), the SPU layers corresponded to a thickness of 210 ± 10 μm. After EPD coating, a change in thickness could not be measured with a digital thickness gauge as no changes were detected. The vast majority (> 95 %) of the prepared SPU surfaces exhibited a porous surface instead of a flat homogeneous surface. Porosity originates from the fast evaporation of the chloroform solvent, which is a stochastic process and therefore the size of the pores is not controlled and was not further investigated as an experiment variable. Fig. 3a shows the SEM micrographs of porous surfaces of two SPU coated SS samples. The micrographs show that the pore size distribution varies from sample to sample. In the first sample, a mean diameter of 3.9 μm was observed while for the second sample a mean pore size of 7.2 μm predominates. Fig. 3b shows an AFM scanning and the profile analysis of a few pores of a third sample showing a

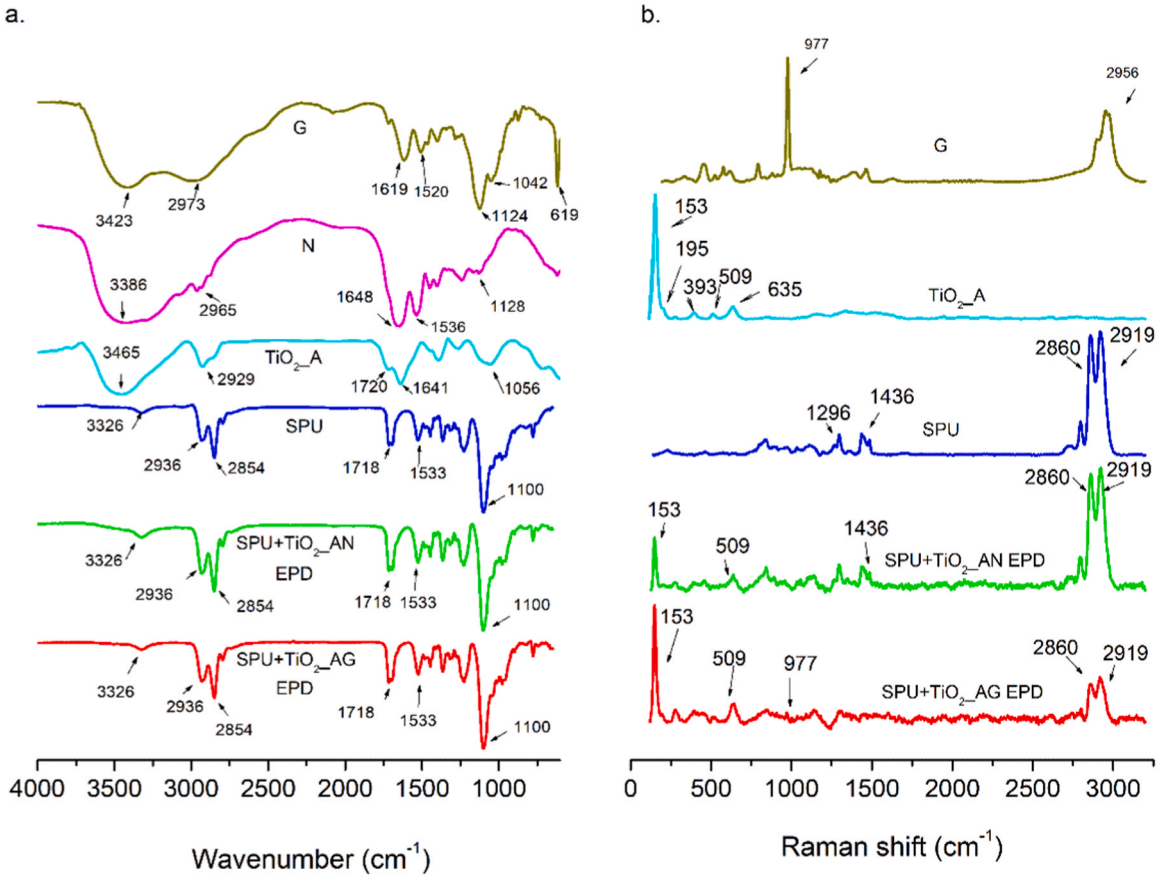

Fig. 2. a. Infrared spectra of samples and **b**. Raman spectra of G (gentamicin powder), N (nisin powder), TiO_2_A (nanotubes powder), SPU (polyurethane layer), SPU+TiO_2_AN (EPD coated SPU with nanotubes and nisin), SPU+TiO_2_AG (EPD coated SPU with nanotubes and gentamicin).

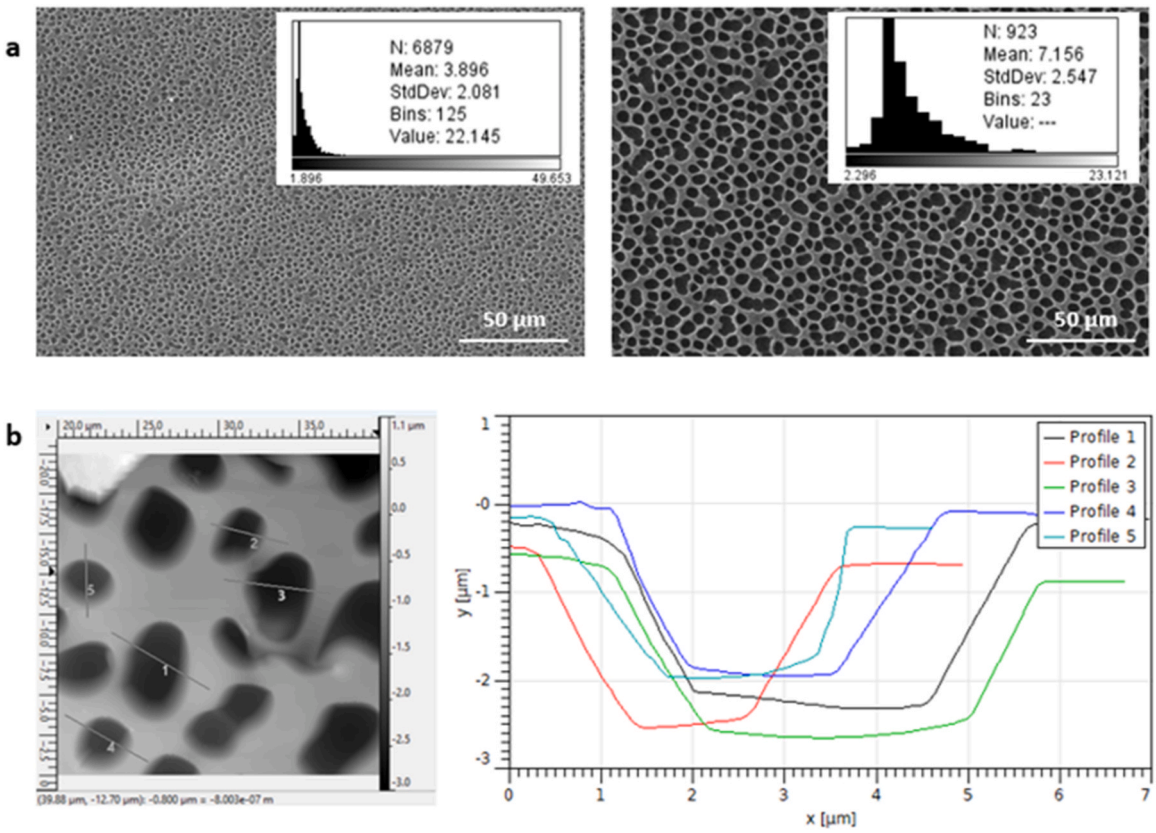

Fig. 3. **a**. SEM micrographs of two different samples of SS 316 L coupons covered with SPU under the same preparation. The in-sets show the distribution size of the pores formed **b**. Profilometry analysis of multiple pores showing a depth of 2.1 ± 0.3 µm.

relatively homogeneous depth of the diameter of 2.1±0.3 µm. Some reports in literature have studied the creation of porous structures in a systematic manner [76,77]. In spite of the lack of control, we believe that this feature will aid the attachment of cells and will promote a better integration with biological entities, as have been reported previously [78,79] In addition, porosity provided more surface area but did not increase the number of deposits as discussed later.

Fig. 4 shows the SEM micrographs of samples with EPD coatings of

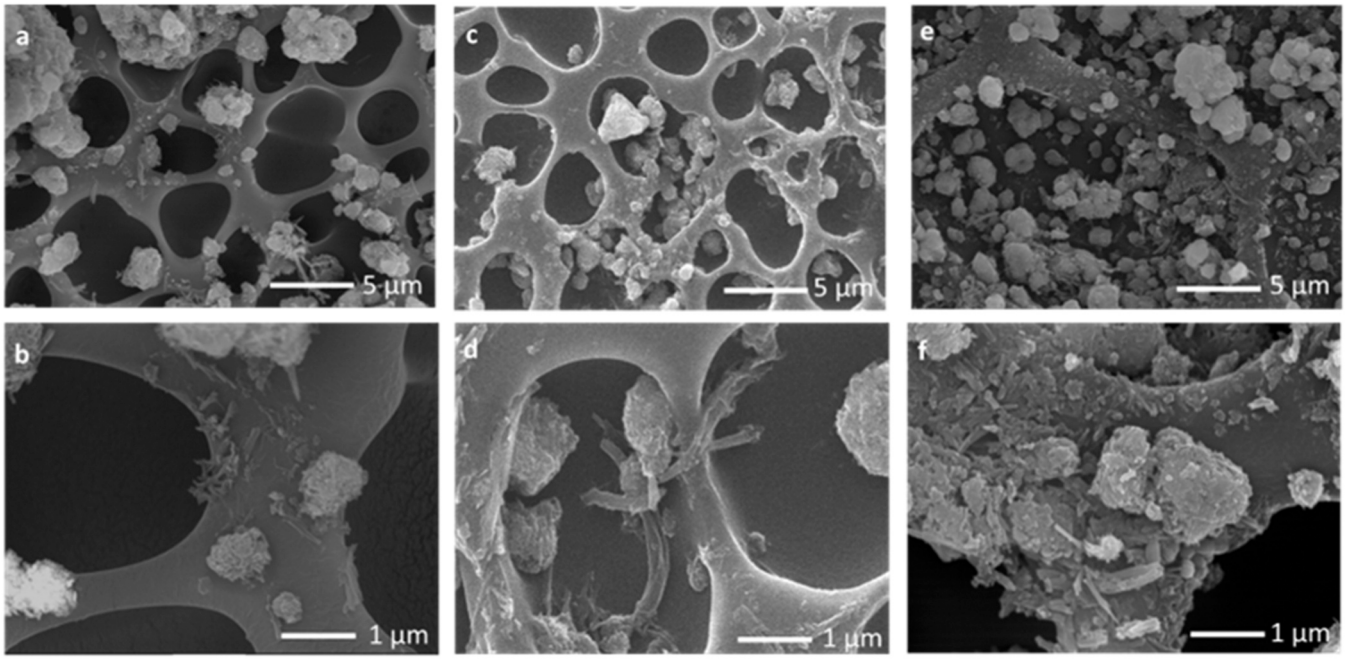

Fig. 4. SEM micrographs at two magnifications of deposits of SPU+TiO_2_A EPD **a** and **b**; deposits of SPU+TiO_2_AG EPD, **c** and **d**; deposits of SPU+TiO_2_AN EPD, **e** and **f**.

SPU+TiO2_A EPD nanotubes and their mixture with antibiotics (SPU+TiO2_AN EPD and SPU+TiO2_AG EPD). We observed that in all cases the particles tend to agglomerate with a few individual nanotubes distributed along the SPU surface. As mentioned before, TiO2_A formed agglomerates before EDP and there is no evidence that it penetrates the SPU coating due to the hydrophobic nature of Tecoflex. The coating takes place both inside and, (predominantly) on the edges of the pores. When N and G are present in the coating, the amount of particles located inside the pores increases. To qualitatively compare the deposits TiO_2 and antibiotics on metal vs metal with SPU coating, EPD was performed on bare SS316L electrodes under the same conditions as the SPU coated coupons. In Figure S4 of the supplemental section, SEM micrographs of the obtained coatings on bare metal are presented. It is noteworthy that the nanotubes TiO2_AG EPD (without SPU) do not form dense coating layers but rather abundant agglomerates that are distributed through the sample. This can be caused by a low zeta potential of TiO_2 that is translated in a low electrophoretic mobility as shown before. The samples TiO2_AG EPD also show the presence of agglomerates similarly to its equivalent sample with SPU, SPU+TiO2_AG EPD. Distinctly, samples TiO2_AN EPD show a different morphology of the nanotube agglomerates where needle-like elongated structures are formed on the metal surface. Meanwhile, SPU+TiO2_AN EPD shows round agglomerates.

From the SEM imaging it is not possible to determine whether gentamicin and nisin are present in the EPD coatings, therefore EDX mapping was performed, and the results shown in Fig. 5a and 5b. The qualitative analysis indicates predominance of C and N which correlate with the polyurethane composition [80] while Ti relates specifically to (TiO_2) nanotube's location, as expected. Oxygen (O) relates to both SPU and TiO_2 since is a main component of both species. Both antibiotics include in their composition S, disulfide bonds in the case of Nisin [81] and sulphate groups in the case of gentamicin; it was observed that sulfur is distributed on all the surface with a slightly higher concentration on the particle location. Additionally, the sample SPU+TiO_2_AN EPD showed the presence of Na and Cl due to salt content in the nisin reagent.

Table 2
Quantitative analysis of prevalent elements on EPD samples.

Element	SPU+TiO_2_AG		SPU+TiO_2_AN	
	Weight%	Atomic%	Weight%	Atomic%
C	46.05	61.55	56.02	70.37
O	32.02	32.13	25.18	23.75
Na	-	-	2.03	1.33
S	0.22	0.11	0.04	0.02
Cl	-	-	2.70	1.15
Ti	16.85	5.65	8.84	2.79
Fe	0.49	0.14	0.78	0.21
Pd	0.91	0.14	0.76	0.11
Au	3.46	0.28	3.64	0.28
Total	100		100.00	

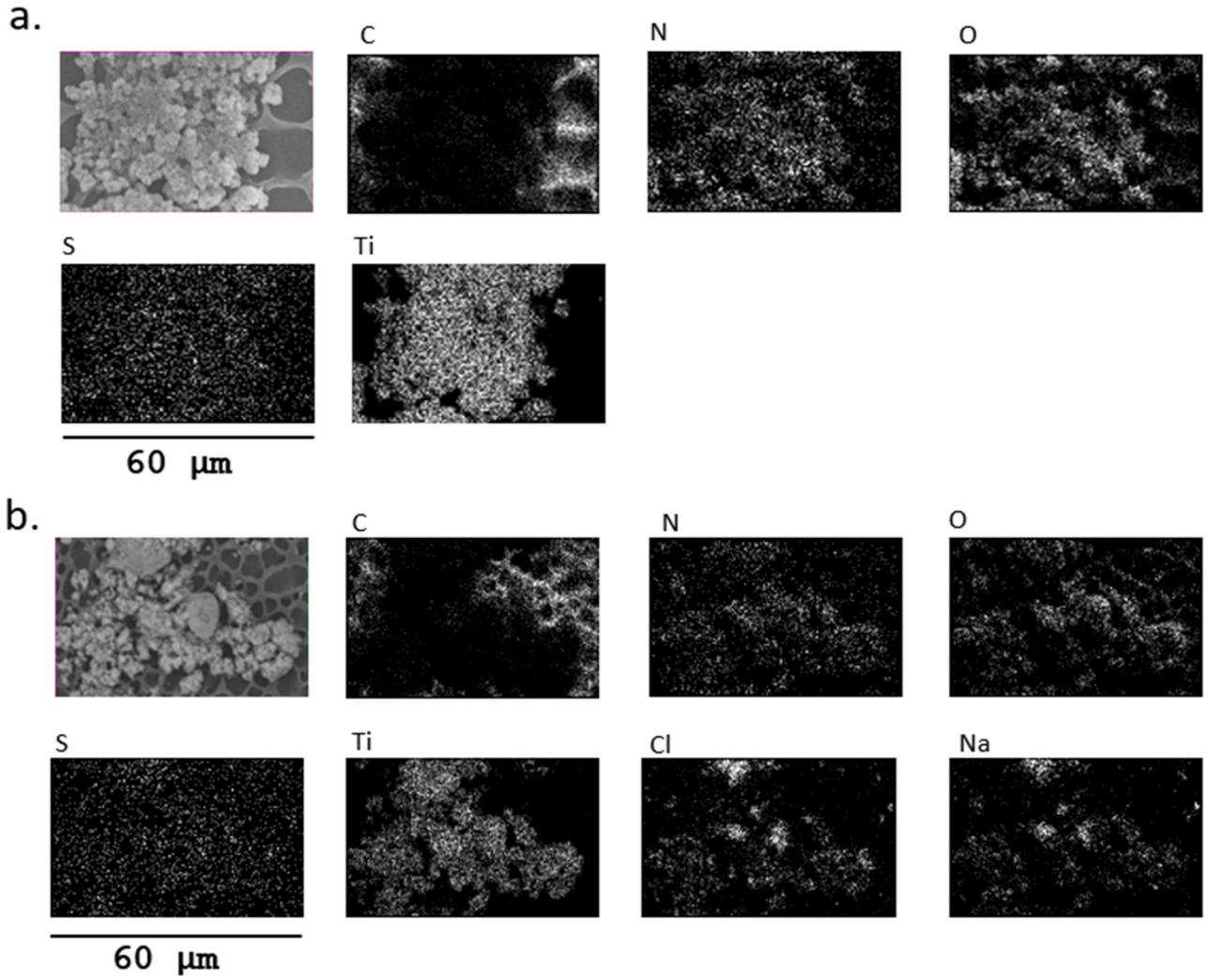

Fig. 5. Overview of prevalent surface elements and mapping of **a**. deposits of SPU+TiO_2_AG EPD and **b**. deposits of SPU+TiO_2_AN EPD.

Quantitative EDX analysis (see Table 2) revealed that the main components of the coating were carbon and oxygen. A relative high concentration of Ti (8–16 wt%) indicated enough deposited particles with a low amount of S (detection of S ≤ 0.2 %). The low percentage of sulphur can be attributed to their low amount of this element on pristine antibiotics (ca. to 5.1 at% and 1.1 at% for gentamicin and nisin respectively). Since samples of SPU+TiO_2_AG EPD and SPU+TiO_2_AN EPD are measured directly on the SS316 L coupons, the presence of Fe is attributed to defects on the SPU layer that allow the beam to reach the 316 L surface and thereby atoms of Fe are detected. Pd and Au are the conducting elements used for samples observation.

AFM was used for the characterization of topography and morphology of EPD coatings. In particular, two channels were selected for imaging, namely topography and phase. The phase contrast imaging principle comes from the monitoring of the shift between the frequency of the AFM cantilever and the driver when tip interacts with the sample surface while topography gives us an indication of depths of pores and height of adhered TiO_2 nanotubes. Phase imaging offers a higher resolution to distinguish coatings since there is a better contrast between materials with different mechanical properties like adhesion, friction, and viscoelasticity [82,83]. Fig. 6 shows representative AFM measurements of topography and phase contrast of SPU+TiO_2_A EPD (a), (b), SPU+TiO_2_AG EPD (c),(d) and SPU+TiO_2_AG EPD (e),(f), coatings. As mentioned earlier, the pores vary in diameter, depth and size depending on the solvent evaporation processes. Measured samples here indicate a minimum in height of −2.0 μm, −1.4 μm and −1.1 μm and a maximum in height of 1.0 μm, 1.8 μm and 1.4 μm for SPU+TiO_2_A EPD, SPU+TiO2_AG EPD and SPU+TiO_2_AN EPD respectively. The phase contrast measurements show the coverage of nanotubes (clearer areas) on the SPU surface (darker areas). Image analysis shows a coverage of ≈17 % of sample area for the SPU+TiO_2_A EPD sample, see Fig. 6b,d,f and Table 3. For the samples with antibiotics the coverage increases up to ≈ 69 % coverage for SPU+TiO_2_AG EPD and ≈ 55 % for SPU+TiO_2_AN EPD. Roughness of samples with nanotubes + antibiotics resulted in higher values of Rq index. It is well known that the surface roughness greatly influences the adhesion of cells on metal surfaces. [79] For instance, osteoblast adhesion and proliferation were driven by the topographic features of etched titanium surfaces, being the samples with higher roughness the ones that performed better.[84] In this sense, the roughness of sample SPU+TiO_2_AG EPD is larger than the roughness of the sample only coated with SPU (see Table 3), therefore, sample SPU+TiO_2_AG EPD provides and adequate surface for cell adhesion.

Due to the sample size and deposit yield, it was challenging to determine the total surface particle density by standard gravimetric methods. Therefore, thermogravimetric analysis (TGA) was performed and reported in Fig. 7, which is a quantitative method with high sensitivity for mass changes [85] The SPU thermogram showed the typical response for Tecoflex© SPU reported elsewhere [40], the weight loss of SPU was of 100 % at 550 °C. TiO_2 particles showed a weight loss of 20 % at 700 °C as similarly shown in literature [86,87] SPU+TiO_2 sample show a shift in the degradation temperature and the residual mass was different from zero (see inset Fig. 7), therefore this mass is directly related to the TiO_2 content. Calculations from the weight loss and the initial mass allowed us to determine the amount of particles initially deposited and thereby the surface density of 140 ± 50 μg/cm^2. Samples with of SPU+TiO_2_A with G and N show a similar behavior as samples

Table 3
AFM parameters of TiO_2 and antibiotics deposited by EPD on SPU coated SS.

Sample	Coverage %	Roughness (Rq, nm)	Maximum height (μm)	Maximum depth (μm)
SPU+TiO_2_A EPD	17±4	75± 40	2.3	-1.9
SPU+TiO_2_AG EPD	69±15	304± 50	1.8	-1.4
SPU+TiO_2_AN EPD	55±5	250± 40	1.7	-1.1
SPU	0	50± 20	0.9	-1.6

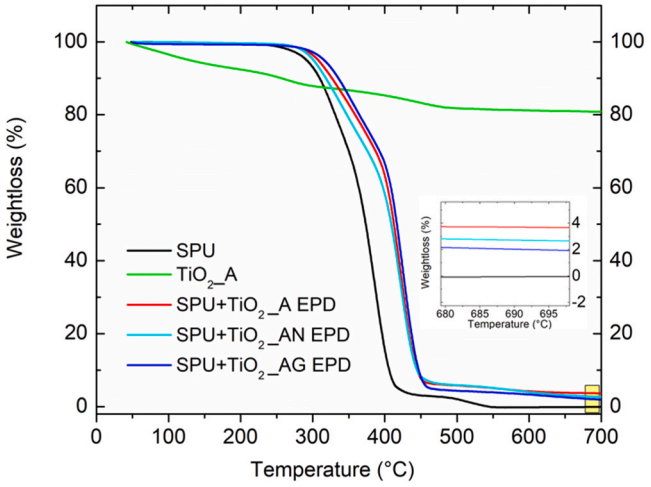

Fig. 7. TGA thermograms of EPD coatings, the inset shows a zoom in of the area highlighted in yellow. SPU and TiO_2_A are samples that correspond to pristine materials.

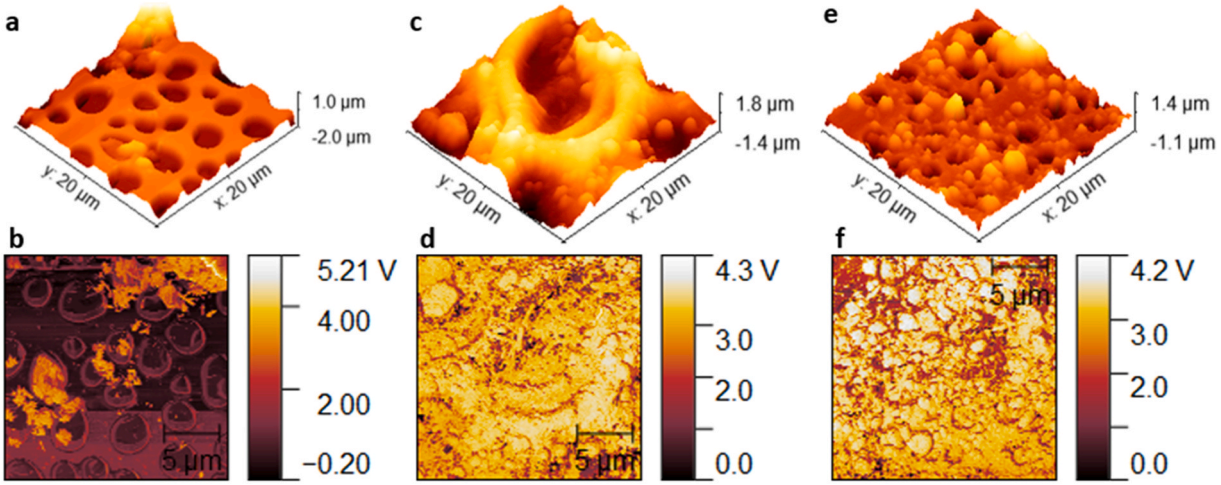

Fig. 6. AFM scans in topography mode (3D) and phase contrast mode respectively for SPU+TiO_2_A EPD **a**, **b**, SPU+TiO_2_AG EPD **c**, **d**, and SPU+TiO_2_AN EPD **e**, **f**.

without. Considering that the residual masses of SPU+TiO_2_AN and SPU+TiO_2_AG samples originate only from the nanotubes and that complete degradation of N and G was achieved at 700 °C, the obtained surface densities of nanotubes were 50 ± 10 μg/cm^2 and 70 ± 50 μg/cm^2 respectively.

Another aspect to look at is the wettability of EPD coatings by the measurement of the contact angle (CA), see Fig. 8. A control sample of bare SPU was measured prior to any treatment and showed a CA of 94 ±5° corresponding to a hydrophobic substrate. The addition of nanotubes has a mild effect in the wetting properties as the contact angle measured is 88°±1°, probably due to a low particle density as being suggested by AFM measurements. In literature the effect of forming a layer of TiO_2 nanoparticles [34] and nanotubes [88] causes an increase in hydrophilicity but in our study, the addition of nisin to the TiO_2 nanotubes increases the hydrophilicity and lowers the CA by 75°±8°, being this effect more dramatic when only nisin is deposited where the CA is 60°±10°. However, Ollé Resa et al. [89] measured the wetting properties of samples with nisin adsorbed surfaces and determined an increment in the CA, in contrast to our findings. On the other hand, gentamicin deposition does not greatly modified SPU wettability as deposits containing TiO_2 and G showed CAs of 94°±1° while for samples where only gentamicin is deposited the CAs was 96°±6°. [81]. For biomedical applications angles between 35° and 80° are acceptable [90] to establish an optimal protein absorption and therefore improved the biocompatibility. Therefore, based on this criterion the sample SPU+TiO_2_AN EPD provides an optimal condition to favor biological interactions.

To evaluate the antibacterial properties of the EPD coating a disk diffusion assay was implemented against *gram-positive S. aureus* and *gram-negative E.coli* (see Fig. 9a,b respectively and Table 4). Since Tecoflex is bioinert, it is thought to not produce antibacterial responses on the coating. TiO_2 nanoparticles are a highly used as additive in medical coatings since they possess antibacterial and non-toxic properties [45]. Therefore, it was interesting to study if there is a synergistic effect by the addition of nisin or gentamicin to the TiO_2 nanoparticles. Discs of SS316L coated with SPU and treated by EPD used as negative control showed no inhibition in both bacterial strains. In contrast, a reference sample of 100 ug of gentamicin impregnated on SPU coated SS3316L (indicated as SPU+G) showed effective inhibition for both strains, which is in line with literature reports [91,92]. Note that EPD suffix is not added to reference samples since they were prepared by simple absorption. Gentamicin had a marked inhibitory response on the *E. coli* agars as it showed 35.7 ± 2.6 mm (see Table 4). Similarly, SPU+TiO_2_AG showed antibacterial inhibition in both strains, which means that gentamicin preserved its antibacterial properties even after voltage application during EPD. TiO_2 nanoparticles in any crystalline phase are a recurred additive for implant coatings due to their antimicrobial properties and the potential to proliferate and grow cells [91]. However, samples with SPU+TiO_2_A and SPU+TiO_2_A EPD did not show any inhibition on any strain. Likewise, reference samples with nisin coatings (indicated as SPU+N) showed a mild inhibitory behavior against *S. aureus* but not against *E. coli*. Even when in literature it is reported the antibacterial properties of nisin against *gram positive* bacteria [93]. Furthermore, samples SPU+TiO_2_AN EPD and SPU+N EPD did not show inhibition in *S. aureus*. The lack of antimicrobial response of nisin could be due to 1) a low concentration of nisin present in the surface and/or 2) denaturation of nisin due to water electrolysis. Seuss et al. [27] and Sikkema et al. [29] discuss the challenge of depositing with EPD proteins, enzymes, and biopolymers. In general, all samples containing gentamicin show inhibitory behavior even after EPD treatment. Some authors have produced hybrid EPD coatings with gentamicin as antibiotic and have reported similar results [94,95]

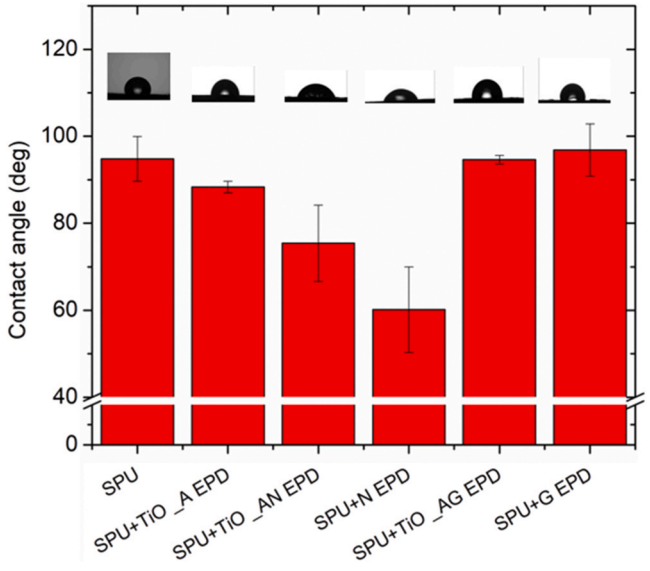

Fig. 8. Contact angle measurements of coatings.

In addition to osteoblasts, fibroblast cells are a key component in the mediation of osseointegration and remolding of soft tissues surrounding the implants, [96] therefore it is essential to study the interaction of coatings obtained by EPD with these cells. To evaluate the cell response, a resazurin cell viability assay on fibroblasts was performed (see Fig. 10). Note that EPD suffix is not added to reference samples since they were prepared by simple absorption. Fig. 10 shows that SPU alone exhibited a viability larger than 90 % after 24 h, which decreases down to to 75 % after 72 h. In addition, samples of SPU+TiO_2_A EPD and SPU+TiO_2_A showed a nontoxic behavior after 72 h and non-significant differences are found respect the SPU (control) sample. Samples with SPU+N EPD show a somewhat reduced viability after 72 h but close to 75 %. Significant differences arise for sample SPU+ N (100 μg of Nisin impregnated) where an initial cytotoxic behavior is measured even at 48 hours; however, viability levels up at 72 hours suggesting that for longer times a higher proliferation can be achieved. Interestingly, when nisin is simultaneously deposited with TiO_2_A (sample SPU+TiO_2_AN EPD), the viability is maintained, and samples become non cytotoxic. In the case of gentamicin loaded samples (SPU +G and SPU+ G EPD) a cytotoxic behavior is observed. However, the toxic effect is minimized when particles and the antibiotic are deposited simultaneously by EPD (sample SPU+TiO_2_AG EPD) where a viability close to 100 % is recovered after 72 h.

4. Conclusions

In this work the coating of metallic supports was carried out. Firstly, a layer of segmented polyurethane was applied. Secondly a mixture of nanotubes of TiO_2 anatase phase and antibiotics (gentamicin and nisin) was deposited by means of electrophoretic deposition. We showed the feasibility of having a SPU nonconductive layer as a substrate for EPD coatings. The addition of a polyurethane coating induced a porous surface for cell adhesion. Preliminary findings also indicate that the Tecoflex coating is an alternative in preventing corrosion and pitting of the SS316L surfaces.

In recent years the need for new types of antibiotics has grown due to bacterial resistance. In this sense, nanoparticle antimicrobial peptides and/or combination with traditional antibiotics have shed light on finding new ways to kill bacteria [97]. In this study, we have shown that the combination of TiO_2_A/Nisin or Gentamicin show interesting features for biological activity. TiO_2_A nanotubes alone deposited with EPD show agglomerates that are distributed all over de SPU layer; TiO_2_AN and TiO_2_AG samples show a larger surface coverage as observed with SEM and AFM. TiO_2_AN samples show an acceptable hydrophilicity range for cellular adhesion. Samples TiO_2_AG performed better in the viability test respect the samples with only gentamicin deposited with

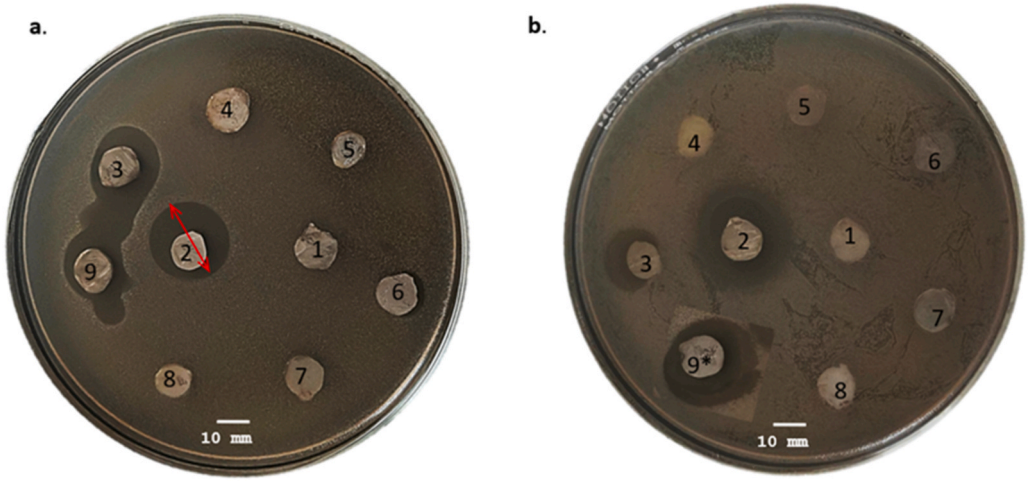

Fig. 9. Antibacterial response of EPD coatings against (a)*S. aureus* (b) *E. coli*. 1: SPU EPD, 2: SPU+G 3: SPU+G EPD, 4: SPU+TiO_2_A, 5: SPU+TiO_2_A EPD, 6: SPU+N, 7: SPU+N EPD, 8: SPU+TiO_2_AN EPD, 9: SPU+TiO_2_AG EPD. The arrow indicates the measurement of the diameters reported in Table 4. * Sample 9 pictures is taken from a different plate.

Table 4
Halo size of samples that showed inhibitory behavior.

Sample	*E. coli* (mm)	*S. aureus* (mm)
SPU+G	35.7 ± 2.6	29.5 ± 2.4
SPU+N	R	17.5 ± 3.0
SPU+G EPD	27.0 ± 5.7	23.3 ± 4.9
SPU+TiO_2_AG EPD	28.3 ± 0.5	21.5 ± 1.0

EPD and by simple absorption. Yet, TiO_2_AG showed antibacterial properties comparable with control sample of only absorbed gentamicin. Therefore, the synergy nanoparticle/antibiotic brings a positive effect on the coating functionality.

One limitation of our approach is the limited yield, and a strategy to increase the deposition rate is by using organic solvents or other types of particles. In this sense, studies with spherical titania nanoparticles are being performed to establish a comparison between the two cases. Another aspect to discuss is the assessment of the biological integrity of the biomolecules under EPD deposition, whereas gentamicin sulphate showed antibacterial properties after EPD treatment, nisin did not exhibit bacterial inhibition. As an alternative, it would be interesting to explore the use of alternating current EPD i.e. the DC electric field is replaced by AC field as it has been suggested to be compatible with all types of biomolecules. Also, the *in vitro* release as well as the minimum inhibitory concentration of antibiotics and nanotubes must be determined to understand the mechanism by which our coatings work and to understand their underlying stability. Finally, the porosity was not controlled here and will be interesting to obtain either a dense coating or to control the pore size by using different solvents and the rate of evaporation.

This research contributes to advancing the utilization of the EPD technique as a valuable method for developing customized coatings with biological activity within the context of metallic implants.

Funding

Thanks to the Consejo Nacional de Humanidades, Ciencias y Tecnologías (CONAHCYT) for funding this project through the posdoctoral grant numbers 332738 (Fabiola Azucena Gutiérrez Mejía) and 637410 (Claudia Vásquez López). Additionally, this research was funded by CONACYT grant number 1360 (Fronteras de la Ciencia) and 248378 (Atención a Problemas Nacionales). Some experiments were conducted at the National Laboratory of Nano and Biomaterials (LANNBIO), CINVESTAV-IPN; funded by the project 322758. This work was also supported by the Ministry of Science, Innovation and Universities of Spain under the grant of the R+D+i project PID2022–137911OB-I00.

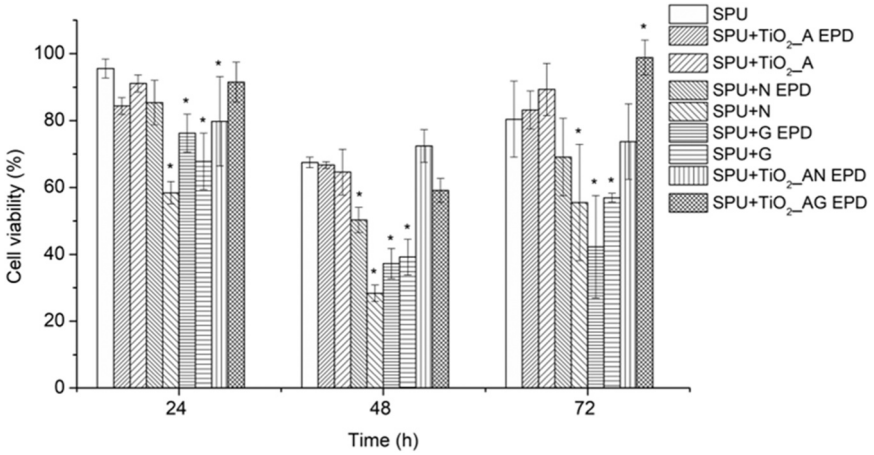

Fig. 10. Viability assay of coatings at 24, 48, and 72 hours.

CRediT authorship contribution statement

Yadir Torres Hernández: Writing – review & editing, Supervision, Funding acquisition. **Juan V. Cauich Rodríguez:** Writing – review & editing, Supervision, Project administration, Funding acquisition, Conceptualization. **Rossana F. Vargas Coronado:** Writing – review & editing, Methodology, Formal analysis. **Fabiola E. Villa de la Torre:** Writing – review & editing, Supervision, Conceptualization. **Fabiola A. Gutiérrez-Mejía:** Writing – original draft, Validation, Supervision, Resources, Methodology, Investigation, Formal analysis, Conceptualization. **Claudia Vásquez López:** Writing – review & editing, Methodology, Formal analysis. **Víctor E. Arana Argaez:** Writing – review & editing, Supervision, Conceptualization. **Ingrid M. Rodríguez Buenfil:** Writing – review & editing, Supervision, Conceptualization. **María M. Gamboa Angulo:** Writing – review & editing, Supervision, Conceptualization.

Declaration of Competing Interest

The authors declare no conflict of interest. The funders had no role in the design of the study; in the collection, analyses, or interpretation of data; in the writing of the manuscript; or in the decision to publish the results.

Data availability

No data was used for the research described in the article.

Acknowledgements

We want to thank Irma Leticia Medina Baizabal and Claribel Huchin Chan for their technical support. Additionally, we want to thank Dr. Francis Avilés Cetina for his support with lab equipment and valuable scientific input. We also want to thank Dr. Patricia Quintana Owen for giving access to LANNBIO. We would like to thank Dr. Máximo Pech-Canul and Dr. Luis Díaz-Ballote from CINVESTAV-IPN Unidad Mérida for their support in corrosion studies.

Appendix A. Supporting information

Supplementary data associated with this article can be found in the online version at doi:10.1016/j.mtcomm.2024.109428.

References

[1] Q. Chen, G.A. Thouas, Metallic implant biomaterials, Mater. Sci. Eng.: R: Rep. 87 (2015) 1–57, https://doi.org/10.1016/J.MSER.2014.10.001.
[2] R. Davis, A. Singh, M.J. Jackson, R.T. Coelho, D. Prakash, C.P. Charalambous, W. Ahmed, L.R.R. da Silva, A.A. Lawrence, A comprehensive review on metallic implant biomaterials and their subtractive manufacturing, Int J. Adv. Manuf. Technol. 120 (2022) 1473–1530, https://doi.org/10.1007/S00170-022-08770-8.
[3] J. Walczak, F. Shahgaldi, F. Heatley, In vivo corrosion of 316L stainless-steel hip implants: morphology and elemental compositions of corrosion products, Biomaterials 19 (1998) 229–237, https://doi.org/10.1016/S0142-9612(97)00208-1.
[4] K. Majid, T. Crowder, E. Baker, K. Baker, D. Koueiter, E. Shields, H.N. Herkowitz, Analysis of in vivo corrosion of 316L stainless steel posterior thoracolumbar plate systems: A retrieval study, J. Spinal Disord. Tech. 24 (2011) 500–505, https://doi.org/10.1097/BSD.0B013E3182064497.
[5] W.H. Goldmann, Biosensitive and antibacterial coatings on metallic material for medical applications, Cell Biol. Int 45 (2021) 1624–1632, https://doi.org/10.1002/CBIN.11604.
[6] T. Fenelon, M. Bakr, L.J. Walsh, R. George, Effects of lasers on titanium dental implant surfaces: a narrative review, 3 6, Lasers Dent. Sci. 6 (2022) (2022) 153–167, https://doi.org/10.1007/S41547-022-00165-Y.
[7] D. Muster, M. Hage-Ali, K.T. Rie, T. Stucky, A. Cornet, D. Mainard, Plasma Deposition, Plasma Coating, and Ion Implantation to Improve Metallic Implants and Prostheses, MRS Bull. 25 (2000) 25–32, https://doi.org/10.1557/S0883769400064988.
[8] J. Liu, N.B. Mohd Rafiq, L.M. Wong, S. Wang, Surface Treatment and Bioinspired Coating for 3D-Printed Implants, Front Chem. 9 (2021) 768007, https://doi.org/10.3389/FCHEM.2021.768007/BIBTEX.
[9] W. Yan, T. Nakamura, M. Kobayashi, H. Kim, F. Miyaji, T. Kokubo, Bonding of chemically treated titanium implants to bone, J. Biomed. Mater. Res 37 (2) (1997) 267–275, https://doi.org/doi:10.1002/(sici)1097-4636(199711).
[10] G. Marenzi, F. Impero, F. Scherillo, J.C. Sammartino, A. Squillace, G. Spagnuolo, Effect of Different Surface Treatments on Titanium Dental Implant Micro-Morphology, 12 (2019) 733, Materials Vol. 12 (2019) 733, https://doi.org/10.3390/MA12050733.
[11] R. Saran, K. Ginjupalli, S.D. George, S. Chidangil, U. V K, LASER as a tool for surface modification of dental biomaterials: A review, Heliyon 9 (2023) e17457, https://doi.org/10.1016/J.HELIYON.2023.E17457.
[12] T. Kokubo, S. Yamaguchi, Bioactive Ti Metal and its Alloys Prepared by Chemical Treatments: State-of-the-Art and Future Trends, Adv. Eng. Mater. 12 (2010) B579–B591, https://doi.org/10.1002/ADEM.201080087.
[13] J. anne N. Oliver, Y. Su, X. Lu, P.H. Kuo, J. Du, D. Zhu, Bioactive glass coatings on metallic implants for biomedical applications, Bioact. Mater. 4 (2019) 261–270, https://doi.org/10.1016/J.BIOACTMAT.2019.09.002.
[14] T. Kumeria, H. Mon, M.S. Aw, K. Gulati, A. Santos, H.J. Griesser, D. Losic, Advanced biopolymer-coated drug-releasing titania nanotubes (TNTs) implants with simultaneously enhanced osteoblast adhesion and antibacterial properties, Colloids Surf. B Biointerfaces 130 (2015) 255–263, https://doi.org/10.1016/J.COLSURFB.2015.04.021.
[15] S. Sharma, V. Gupta, D. Mudgal, Current trends, applications, and challenges of coatings on additive manufacturing based biopolymers: A state of art review, Polym. Compos 43 (2022) 6749–6781, https://doi.org/10.1002/PC.26809.
[16] W.S.W. Harun, R.I.M. Asri, J. Alias, F.H. Zulkifli, K. Kadirgama, S.A.C. Ghani, J.H. M. Shariffuddin, A comprehensive review of hydroxyapatite-based coatings adhesion on metallic biomaterials, Ceram. Int 44 (2018) 1250–1268, https://doi.org/10.1016/J.CERAMINT.2017.10.162.
[17] N. Wang, J.Y.H. Fuh, S.T. Dheen, A. Senthil Kumar, Functions and applications of metallic and metallic oxide nanoparticles in orthopedic implants and scaffolds, J. Biomed. Mater. Res B Appl. Biomater. 109 (2021) 160–179, https://doi.org/10.1002/JBM.B.34688.
[18] F. Tosan, A.H. Fathi, A. Yari, N. Rahnama, D. Sakhaei, Effects of doping metal nanoparticles in hydroxyapatite in Improving the physical and chemical properties of dental implants, Nanomed. Res. J. 6 (2021) 327–336, https://doi.org/10.22034/NMRJ.2021.04.002.
[19] T.V. Basova, E.S. Vikulova, S.I. Dorovskikh, A. Hassan, N.B. Morozova, The use of noble metal coatings and nanoparticles for the modification of medical implant materials, Mater. Des. 204 (2021) 109672, https://doi.org/10.1016/J.MATDES.2021.109672.
[20] A. Agrelli, N.F. Vasconcelos, R.C.S. da Silva, C.L. Mendes-Marques, I.R. de S. Arruda, P.S.S. de Oliveira, L.R.L. Santos, A.N. de Andrade, R.R. de Moura, L. C. Bernardo-Menezes, N.P. da Silva, G. Machado, Peptides for Coating TiO2 Implants: An In Silico Approach, Int J. Mol. Sci. 23 (2022), https://doi.org/10.3390/IJMS232214048.
[21] C.L. Romanò, S. Scarponi, E. Gallazzi, D. Romanò, L. Drago, Antibacterial coating of implants in orthopaedics and trauma: a classification proposal in an evolving panorama, 1 10, J. Orthop. Surg. Res. 10 (2015) (2015) 1–11, https://doi.org/10.1186/S13018-015-0294-5.
[22] J.M. Schierholz, J. Beuth, Implant infections: a haven for opportunistic bacteria, J. Hosp. Infect. 49 (2001) 87–93, https://doi.org/10.1053/JHIN.2001.1052.
[23] C.R. Arciola, D. Campoccia, L. Montanaro, Implant infections: adhesion, biofilm formation and immune evasion, 7 16, Nat. Rev. Microbiol. 16 (2018) (2018) 397–409, https://doi.org/10.1038/s41579-018-0019-y.
[24] S. Arango, A. Peláez-Vargas, C. García, Coating and Surface Treatments on Orthodontic Metallic Materials, 3 (2012) 1–15, Coatings Vol. 3 (2013) 1–15, https://doi.org/10.3390/COATINGS3010001.
[25] A. Dehghanghadikolaei, B. Fotovvati, Coating Techniques for Functional Enhancement of Metal Implants for Bone Replacement: A Review, 12 (2019) 1795, Materials Vol. 12 (2019) 1795, https://doi.org/10.3390/MA12111795.
[26] P.C. Innocenzi, M. Guglielmi, M. Gobbin, P. Colombo, Coating of metals by the sol-gel dip-coating method, J. Eur. Ceram. Soc. 10 (1992) 431–436, https://doi.org/10.1016/0955-2219(92)90018-9.
[27] S. Seuss, A.R. Boccaccini, Electrophoretic deposition of biological macromolecules, drugs, and cells, Biomacromolecules 14 (2013) 3355–3369, https://doi.org/10.1021/bm401021b.
[28] T. Yoshioka, A. Chávez-Valdez, J.A. Roether, D.W. Schubert, A.R. Boccaccini, AC electrophoretic deposition of organic-inorganic composite coatings, J. Colloid Interface Sci. 392 (2013) 167–171, https://doi.org/10.1016/j.jcis.2012.09.087.
[29] R. Sikkema, K. Baker, I. Zhitomirsky, Electrophoretic deposition of polymers and proteins for biomedical applications, Adv. Colloid Interface Sci. 284 (2020) 102272, https://doi.org/10.1016/j.cis.2020.102272.
[30] A. Błoniarz, K. Cholewa-Kowalska, M. Gajewska, B. Grysakowski, T. Moskalewicz, Electrophoretic deposition, microstructure and selected properties of nanocrystalline SnO2/Sr enriched bioactive glass/chitosan composite coatings on titanium, Surf. Coat. Technol. 450 (2022) 129004, https://doi.org/10.1016/J.SURFCOAT.2022.129004.
[31] K.S. Akshay, V.P.M. Rabeeh, S.A. Rahim, K.P. Sijina, G.K. Rajanikant, T. Hanas, Electrophoretic deposition of alginate/bioglass composite coating on MgCa alloy for degradable metallic implant applications, Surf. Coat. Technol. 448 (2022) 128914, https://doi.org/10.1016/J.SURFCOAT.2022.128914.
[32] S. Tang, B. Tian, Y.J. Guo, Z.A. Zhu, Y.P. Guo, Chitosan/carbonated hydroxyapatite composite coatings: Fabrication, structure and biocompatibility, Surf. Coat. Technol. 251 (2014) 210–216, https://doi.org/10.1016/J.SURFCOAT.2014.04.028.

[33] K. Grandfield, I. Zhitomirsky, Electrophoretic deposition of composite hydroxyapatite-silica-chitosan coatings, Mater. Charact. 59 (2008) 61–67, https://doi.org/10.1016/j.matchar.2006.10.016.
[34] L. Cordero-Arias, S. Cabanas-Polo, H. Gao, J. Gilabert, E. Sanchez, J.A. Roether, D. W. Schubert, S. Virtanen, A.R. Boccaccini, Electrophoretic deposition of nanostructured-TiO2/chitosan composite coatings on stainless steel, RSC Adv. 3 (2013) 11247–11254, https://doi.org/10.1039/C3RA40535D.
[35] Z. Hadzhieva, A.R. Boccaccini, Recent developments in electrophoretic deposition (EPD) of antibacterial coatings for biomedical applications - A review, Curr. Opin. Biomed. Eng. 21 (2022) 100367, https://doi.org/10.1016/J.COBME.2021.100367.
[36] M.A.U. Rehman, S.A. Batool, Development of sustainable antibacterial coatings based on electrophoretic deposition of multilayers: gentamicin-loaded chitosan/gelatin/bioactive glass deposition on PEEK/bioactive glass layer, Int. J. Adv. Manuf. Technol. 120 (2022) 3885–3900, https://doi.org/10.1007/S00170-022-09024-3/METRICS.
[37] T. Aydemir, L. Liverani, J.I. Pastore, S.M. Ceré, W.H. Goldmann, A.R. Boccaccini, J. Ballarre, Functional behavior of chitosan/gelatin/silica-gentamicin coatings by electrophoretic deposition on surgical grade stainless steel, Mater. Sci. Eng.: C. 115 (2020) 111062, https://doi.org/10.1016/J.MSEC.2020.111062.
[38] M. Bartmański, Ł. Pawłowski, A. Zieliński, A. Mielewczyk-Gryń, G. Strugała, B. Cieślik, Electrophoretic Deposition and Characteristics of Chitosan–Nanosilver Composite Coatings on a Nanotubular TiO2 Layer, 10 (2020) 245, Coatings Vol. 10 (2020) 245, https://doi.org/10.3390/COATINGS10030245.
[39] H. Shaygani, S. Seifi, A. Shamloo, M. Golizadeh, S.Y. Rahnamaee, M. Alishiri, S. Ebrahimi, Novel bilayer coating on gentamicin-loaded titanium nanotube for orthopedic implants applications, Int J. Pharm. 636 (2023) 122764, https://doi.org/10.1016/J.IJPHARM.2023.122764.
[40] J.C. Audifred-Aguilar, V.H. Pino-Ramos, E. Bucio, Synthesis and characterization of hydrophilically modified Tecoflex® polyurethane catheters for drug delivery, Mater. Today Commun. 26 (2021) 101894, https://doi.org/10.1016/J.MTCOMM.2020.101894.
[41] H. Isayama, Y. Komatsu, T. Tsujino, H. Yoshida, M. Tada, Y. Shiratori, T. Kawabe, M. Omata, Polyurethane-covered metal stent for management of distal malignant biliary obstruction, Gastrointest. Endosc. 55 (2002) 366–370, https://doi.org/10.1067/mge.2002.121876.
[42] M.M. Mazumder, S. De, S. Trigwell, N. Ali, M.K. Mazumder, J.L. Mehta, Corrosion resistance of polyurethane-coated Nitinol cardiovascular stents, J. Biomater. Sci. Polym. Ed. 14 (2003) 1351–1362, https://doi.org/10.1163/156856203322599699.
[43] M. Yadav, J.K. Saha, S.K. Ghosh, Surface, Chemical, and Mechanical Properties of Polyurethane-Coated Galvanized Steel Sheets, J. Mater. Eng. Perform. (2024) 1–16, https://doi.org/10.1007/s11665-024-09171-6.
[44] F.M. de Souza, R.K. Gupta, Waterborne Polyurethanes for Corrosion Protection, Adv. Sci., Technol. Innov. (2021) 1–27, https://doi.org/10.1007/978-3-030-72869-4_1.
[45] K. Lingaraju, R.B. Basavaraj, K. Jayanna, S. Bhavana, S. Devaraja, H.M. Kumar Swamy, G. Nagaraju, H. Nagabhushana, H. Raja Naika, Biocompatible fabrication of TiO2 nanoparticles: Antimicrobial, anticoagulant, antiplatelet, direct hemolytic and cytotoxicity properties, Inorg. Chem. Commun. 127 (2021) 108505, https://doi.org/10.1016/J.INOCHE.2021.108505.
[46] L. Liu, R. Bhatia, T.J. Webster, Atomic layer deposition of nano-TiO2 thin films with enhanced biocompatibility and antimicrobial activity for orthopedic implants, Int J. Nanomed. 12 (2017) 8711–8723, https://doi.org/10.2147/IJN.S148065.
[47] L. Zhang, Z. Jin, Antibacterial activities of titanium dioxide (TiO2) nanotube with planar titanium silver (TiAg) to prevent orthopedic implant infection, J. Orthop. Surg. Res 19 (2024) 1–8, https://doi.org/10.1186/s13018-024-04596-0.
[48] A. Radtke, A. Topolski, T. Jędrzejewski, W. Kozak, B. Sadowska, M. Więckowska-Szakiel, P. Piszczek, Bioactivity Studies on Titania Coatings and the Estimation of Their Usefulness in the Modification of Implant Surfaces, 7 (2017) 90, Nanomaterials Vol. 7 (2017) 90, https://doi.org/10.3390/NANO7040090.
[49] L.J. de Arauz, A.F. Jozala, P.G. Mazzola, T.C. Vessoni Penna, Nisin biotechnological production and application: a review, Trends Food Sci. Technol. 20 (2009) 146–154, https://doi.org/10.1016/j.tifs.2009.01.056.
[50] M. Hage, N.E. Chihib, M. Abdallah, S. Khelissa, B. Crocco, H. Akoum, F. Bentiss, C. Jama, Nisin-based coatings for the prevention of biofilm formation: Surface characterization and antimicrobial assessments, Surf. Interfaces 27 (2021) 101564, https://doi.org/10.1016/j.surfin.2021.101564.
[51] Z. Tong, L. Ni, J. Ling, Antibacterial peptide nisin: A potential role in the inhibition of oral pathogenic bacteria, Pept. (N. Y.) 60 (2014) 32–40, https://doi.org/10.1016/j.peptides.2014.07.020.
[52] J.M. Shin, J.W. Gwak, P. Kamarajan, J.C. Fenno, A.H. Rickard, Y.L. Kapila, Biomedical applications of nisin, J. Appl. Microbiol 120 (2016) 1449–1465, https://doi.org/10.1111/JAM.13033.
[53] V. Alessandra Gobbo, M. Lallukka, F. Gamna, M. Prato, A. Vitale, S. Ferraris, Z. Najmi, A. Cochis, L. Rimondini, J. Massera, S. Spriano, Functionalization of a chemically treated Ti6Al4V-ELI alloy with nisin for antibacterial purposes, Appl. Surf. Sci. 620 (2023) 156820, https://doi.org/10.1016/J.APSUSC.2023.156820.
[54] J. Sojo-Dorado, J. Rodríguez-Baño, Gentamicin, Kucers the Use of Antibiotics: A Clinical Review of Antibacterial, Antifungal, Antiparasitic, and Antiviral Drugs, Seven-.-. Ed. (2023) 964–991, https://doi.org/10.1201/9781315152110.
[55] Kirby-Bauer Disk Diffusion Susceptibility Test Protocol | ASM.org, (n.d.). ⟨https://asm.org/protocols/kirby-bauer-disk-diffusion-susceptibility-test-pro⟩ (accessed November 17, 2023).
[56] Measuring cytotoxicity or proliferation - alamarBlue Assay Protocol | Bio-Rad, (n.d.). ⟨https://www.bio-rad-antibodies.com/measuring-cytotoxicity-proliferation-spectrophotometry-fluorescence-alamarBlue.html⟩ (accessed November 21, 2023).
[57] X. Cheng, Y. Liu, O. Liu, Y. Lu, Z. Liao, Z. Hadzhieva, L. Chen, S.G. C. Leeuwenburgh, A.R. Boccaccini, F. Yang, Electrophoretic deposition of coatings for local delivery of therapeutic agents, Prog. Mater. Sci. 136 (2023) 101111, https://doi.org/10.1016/J.PMATSCI.2023.101111.
[58] E.A. Davies, H.E. Bevis, R. Potter, J. Harris, G.C. Williams, J. Delves-Broughton, Research note: The effect of pH on the stability of nisin solution during autoclaving, Lett. Appl. Microbiol 27 (1998) 186–187, https://doi.org/10.1046/J.1472-765X.1998.T01-1-00401.X.
[59] B.E. Rosenkrantz, J.R. Greco, J.G. Hoogerheide, E.M. Oden, Gentamicin Sulfate, Anal. Profiles Drug Subst. Excip. 9 (1981) 295–340, https://doi.org/10.1016/S0099-5428(08)60145-8.
[60] S. Dor, S. Rühle, A. Ofir, M. Adler, L. Grinis, A. Zaban, The influence of suspension composition and deposition mode on the electrophoretic deposition of TiO2 nanoparticle agglomerates, Colloids Surf. A Physicochem Eng. Asp. 342 (2009) 70–75, https://doi.org/10.1016/J.COLSURFA.2009.04.009.
[61] L. Brabec, Quantitative electrophoretic deposition (Q-EPD) of TiO2 nanopowders, Mater. Lett. 333 (2023) 133620, https://doi.org/10.1016/J.MATLET.2022.133620.
[62] A.K. Van Helden, J.W. Jansen, A. Vrij, Preparation and characterization of spherical monodisperse silica dispersions in nonaqueous solvents, J. Colloid Interface Sci. 81 (1981) 354–368, https://doi.org/10.1016/0021-9797(81)90417-3.
[63] C. Nyby, X. Guo, J.E. Saal, S.C. Chien, A.Y. Gerard, H. Ke, T. Li, P. Lu, C. Oberdorfer, S. Sahu, S. Li, C.D. Taylor, W. Windl, J.R. Scully, G.S. Frankel, Electrochemical metrics for corrosion resistant alloys, Sci. Data 8 (2021) 58, https://doi.org/10.1038/S41597-021-00840-Y.
[64] H. Liao, M. Wu, D. Deng, W. Zhong, B. Xiong, Y. Tong, Effects of Ti content on the microstructure, mechanical properties and corrosion behavior of TixZrNb alloys, J. Mater. Res. Technol. 19 (2022) 1433–1443, https://doi.org/10.1016/J.JMRT.2022.05.140.
[65] P.M. Vilarinho, Z. Fu, A. Wu, A. Axelsson, A.I. Kingon, Electrophoretic deposition on nonconducting substrates: A demonstration of the application to microwave devices, Langmuir 31 (2015) 2127–2135, https://doi.org/10.1021/la504184k.
[66] P. Zhao, L.J. LeSergent, J. Farnese, J.Z. Wen, C.L. Ren, Electrophoretic deposition of carbon nanotubes on semi-conducting and non-conducting substrates, Electrochem Commun. 108 (2019) 106558, https://doi.org/10.1016/J.ELECOM.2019.106558.
[67] L. Besra, M. Liu, A review on fundamentals and applications of electrophoretic deposition (EPD), Prog. Mater. Sci. 52 (2007) 1–61, https://doi.org/10.1016/J.PMATSCI.2006.07.001.
[68] A. Arakkal, P. Sirajunnisa, G.S. Sailaja, Natural rubber latex films with effective growth inhibition against S. aureus via surface conjugated gentamicin, J. Bioact. Compat. Polym. 38 (2023) 220–233, https://doi.org/10.1177/08839115231153823.
[69] C. Dwivedi, H. Pandey, A.C. Pandey, P.W. Ramteke, Fabrication and Assessment of Gentamicin Loaded Electrospun Nanofibrous Scaffolds as a Quick Wound Healing Dressing Material, Curr. Nanosci. 11 (2015) 222–228.
[70] A. León, P. Reuquen, C. Garín, R. Segura, P. Vargas, P. Zapata, P.A. Orihuela, FTIR and Raman Characterization of TiO2 Nanoparticles Coated with Polyethylene Glycol as Carrier for 2-Methoxyestradiol, 7 (2017) 49, Appl. Sci. Vol. 7 (2017) 49, https://doi.org/10.3390/APP7010049.
[71] C. Guignot, N. Betz, B. Legendre, A. Le Moel, N. Yagoubi, Degradation of segmented poly(etherurethane) Tecoflex® induced by electron beam irradiation: Characterization and evaluation, Nucl. Instrum. Methods Phys. Res B 185 (2001) 100–107, https://doi.org/10.1016/S0168-583X(01)00850-3.
[72] S. Zaleski, K.A. Clark, M.M. Smith, J.Y. Eilert, M. Doty, R.P. Van Duyne, Identification and Quantification of Intravenous Therapy Drugs Using Normal Raman Spectroscopy and Electrochemical Surface-Enhanced Raman Spectroscopy, Anal. Chem. 89 (2017) 2497–2504, https://doi.org/10.1021/acs.analchem.6b04636.
[73] A. Tryfon, P. Siafarika, C. Kouderis, S. Kaziannis, S. Boghosian, A.G. Kalampounias, Evidence of Self-Association and Conformational Change in Nisin Antimicrobial Polypeptide Solutions: A Combined Raman and Ultrasonic Relaxation Spectroscopic and Theoretical Study, 12 (2023) 221, Antibiotics Vol. 12 (2023) 221, https://doi.org/10.3390/ANTIBIOTICS12020221.
[74] S.S. El-Deen, A.M. Hashem, A.E. Abdel Ghany, S. Indris, H. Ehrenberg, A. Mauger, C.M. Julien, Anatase TiO2 nanoparticles for lithium-ion batteries, Ion. (Kiel.) 24 (2018) 2925–2934, https://doi.org/10.1007/S11581-017-2425-Y.
[75] J. Macossay, F.A. Sheikh, T. Cantu, T.M. Eubanks, M.E. Salinas, C.S. Farhangi, H. Ahmad, M.S. Hassan, M.S. Khil, S.K. Maffi, H. Kim, G.L. Bowlin, Imaging, spectroscopic, mechanical and biocompatibility studies of electrospun Tecoflex® EG 80A nanofibers and composites thereof containing multiwalled carbon nanotubes, Appl. Surf. Sci. 321 (2014) 205–213, https://doi.org/10.1016/J.APSUSC.2014.09.198.
[76] Y. Fu, M. Soldera, W. Wang, S. Milles, K. Deng, B. Voisiat, K. Nielsch, A.F. Lasagni, Wettability control of polymeric microstructures replicated from laser-patterned stamps, 1 10, Sci. Rep. 10 (2020) (2020) 1–11, https://doi.org/10.1038/s41598-020-79936-1.
[77] C. Ge, W. Zhai, Cellular Thermoplastic Polyurethane Thin Film: Preparation, Elasticity, and Thermal Insulation Performance, Ind. Eng. Chem. Res 57 (2018) 4688–4696, https://doi.org/10.1021/acs.iecr.7b05037.
[78] M. Kiremitçi, M. Pulat, C. Şenvar, A.I. Şerbetçi, E. Pişkin, Structural and cellular characterization of solvent-casted polyurethane membranes, Clin. Mater. 6 (1990) 227–237, https://doi.org/10.1016/0267-6605(90)90060-9.

[79] J.L. Hernandez, K.A. Woodrow, Medical applications of porous biomaterials: features of porosity and tissue-specific implications for biocompatibility, Adv. Health Mater. 11 (2022) e2102087, https://doi.org/10.1002/ADHM.202102087.
[80] Tecoflex | C43H76N4O8 | CID 3086063 - PubChem, (n.d.). ⟨https://pubchem.ncbi.nlm.nih.gov/compound/Tecoflex#section=Related-Records⟩ (accessed October 21, 2023).
[81] H.S. Rollema, O.P. Kuipers, P. Both, W.M. De Vos, R.J. Siezen, Improvement of Solubility and Stability of the Antimicrobial Peptide Nisin by Protein Engineering, Appl. Environ. Microbiol 61 (1995) 2873–2878.
[82] S. Bhaduri, S. Mallick, N. Shiradkar, A. Kottantharayil, Characterization of reliability of anti-soiling coatings using tapping mode-AFM phase imaging, J. Renew. Sustain. Energy 13 (2021), https://doi.org/10.1063/5.0039255/1058446.
[83] G.K.H. Pang, K.Z. Baba-Kishi, A. Patel, Topographic and phase-contrast imaging in atomic force microscopy, Ultramicroscopy 81 (2000) 35–40, https://doi.org/10.1016/S0304-3991(99)00164-3.
[84] J.I. Rosales-Leal, M.A. Rodríguez-Valverde, G. Mazzaglia, P.J. Ramón-Torregrosa, L. Díaz-Rodríguez, O. García-Martínez, M. Vallecillo-Capilla, C. Ruiz, M. A. Cabrerizo-Vílchez, Effect of roughness, wettability and morphology of engineered titanium surfaces on osteoblast-like cell adhesion, Colloids Surf. A Physicochem Eng. Asp. 365 (2010) 222–229, https://doi.org/10.1016/J.COLSURFA.2009.12.017.
[85] N. Saadatkhah, A. Carillo Garcia, S. Ackermann, P. Leclerc, M. Latifi, S. Samih, G. S. Patience, J. Chaouki, Experimental methods in chemical engineering: Thermogravimetric analysis—TGA, Can. J. Chem. Eng. 98 (2020) 34–43, https://doi.org/10.1002/CJCE.23673.
[86] S.S. Al-Taweel, H.R. Saud, A.A.H. Kadhum, M.S. Takriff, The influence of titanium dioxide nanofiller ratio on morphology and surface properties of TiO2/chitosan nanocomposite, Results Phys. 13 (2019) 102296, https://doi.org/10.1016/J.RINP.2019.102296.
[87] S. Balaji, R. Guda, B.K. Mandal, M. Kasula, E. Ubba, F.R.N. Khan, Green synthesis of nano-titania (TiO2 NPs) utilizing aqueous Eucalyptus globulus leaf extract: applications in the synthesis of 4H-pyran derivatives, Res. Chem. Intermed. 47 (2021) 3919–3931, https://doi.org/10.1007/s11164-018-03720-0.
[88] E. Balaur, J.M. MacAk, L. Taveira, P. Schmuki, Tailoring the wettability of TiO2 nanotube layers, Electrochem Commun. 7 (2005) 1066–1070, https://doi.org/10.1016/J.ELECOM.2005.07.014.
[89] C.P. Ollé Resa, R.J. Jagus, L.N. Gerschenson, Effect of natamycin, nisin and glycerol on the physicochemical properties, roughness and hydrophobicity of tapioca starch edible films, Mater. Sci. Eng.: C. 40 (2014) 281–287, https://doi.org/10.1016/J.MSEC.2014.04.005.
[90] J.H. Lee, G. Khang, J.W. Lee, H.B. Lee, Interaction of Different Types of Cells on Polymer Surfaces with Wettability Gradient, J. Colloid Interface Sci. 205 (1998) 323–330, https://doi.org/10.1006/JCIS.1998.5688.
[91] V.H. Tam, S. Kabbara, G. Vo, A.N. Schilling, E.A. Coyle, Comparative pharmacodynamics of gentamicin against Staphylococcus aureus and Pseudomonas aeruginosa, Antimicrob. Agents Chemother. 50 (2006) 2626–2631, https://doi.org/10.1128/aac.01165-05.
[92] F. Husen, N.I. Ratnaningtyas, Inhibitory Test of Gentamicin Antibiotics Against Escherichia coli and Staphylococcus aureus Bacteria Using Disc Method, Biotropika: J. Trop. Biol. 10 (2022) 126–131, https://doi.org/10.21776/UB.BIOTROPIKA.2022.010.02.06.
[93] K. Kuwano, N. Tanaka, T. Shimizu, K. Nagatoshi, S. Nou, K. Sonomoto, Dual antibacterial mechanisms of nisin Z against Gram-positive and Gram-negative bacteria, Int J. Antimicrob. Agents 26 (2005) 396–402, https://doi.org/10.1016/J.IJANTIMICAG.2005.08.010.
[94] M. Stevanović, M. Došić, A. Janković, V. Kojić, M. Vukašinović-Sekulić, J. Stojanović, J. Odović, M. Crevar Sakač, K.Y. Rhee, V. Mišković-Stanković, Gentamicin-Loaded Bioactive Hydroxyapatite/Chitosan Composite Coating Electrodeposited on Titanium, ACS Biomater. Sci. Eng. 4 (2018) 3994–4007, https://doi.org/10.1021/acsbiomaterials.8b00859.
[95] F. Pishbin, V. Mouriño, S. Flor, S. Kreppel, V. Salih, M.P. Ryan, A.R. Boccaccini, Electrophoretic deposition of gentamicin-loaded bioactive glass/chitosan composite coatings for orthopaedic implants, ACS Appl. Mater. Interfaces 6 (2014) 8796–8806, https://doi.org/10.1021/am5014166.
[96] X. Hu, K.G. Neoh, Z. Shi, E.T. Kang, W. Wang, An In Vitro Assessment of Fibroblast and Osteoblast Response to Alendronate-Modified Titanium and the Potential for Decreasing Fibrous Encapsulation, Tissue Eng. Part A 19 (2013) 1919, https://doi.org/10.1089/TEN.TEA.2012.0218.
[97] A. León-Buitimea, C.R. Garza-Cárdenas, J.A. Garza-Cervantes, J.A. Lerma-Escalera, J.R. Morones-Ramírez, The Demand for New Antibiotics: Antimicrobial Peptides, Nanoparticles, and Combinatorial Therapies as Future Strategies in Antibacterial Agent Design, Front Microbiol 11 (2020) 551136, https://doi.org/10.3389/fmicb.2020.01669.